Evolution of the conducting phase topology at the percolation threshold in colossal magnetoresistance manganites: A magnetic small-angle neutron scattering study

Damien Saurel,[1] Charles Simon,[1,*] Alain Pautrat,[1] Christine Martin,[1] Charles Dewhurst,[2] and Annie Brûlet[3]
[1]*Laboratoire CRISMAT, UMR 6508 CNRS, ENSICAEN, 14050 Caen, France*
[2]*Institut Laue Langevin, BP 156, 38042 Grenoble Cedex 9, France*
[3]*Laboratoire Léon Brillouin, UMR 12 CEA CNRS, CEA Saclay, 91191 Gif-sur-Yvette, France*
(Received 15 April 2009; published 25 August 2010)

We have studied by small-angle neutron scattering the magnetic field evolution of the magnetic phase separation in a colossal magnetoresistive (CMR) $Pr_{0.7}Ca_{0.3}MnO_3$ crystal, in a wide range of scattering vectors Q, down to 2×10^{-3} Å^{-1} and up to 10^{-1} Å^{-1}. Access to such small Q values allows measuring the Q^{-4} scattering from interfaces between ferromagnetic and antiferromagnetic phases appearing along the phase separation. We were able to monitor its evolution from the very beginning of the insulator-to-metal transition, characteristic of the CMR effect. Our results confirm the percolation scenario of a field-induced conducting phase of micrometric size growing within the initial antiferromagnetic insulating phase. Moreover, we show that the CMR transition occurs when the transformation mechanism starts to be driven by large-scale strain field minimization.

DOI: 10.1103/PhysRevB.82.054427 PACS number(s): 75.47.Gk, 75.47.Lx, 75.30.Kz, 71.30.+h

I. INTRODUCTION

The mixed valence $A_{1-x}B_xMnO_3$ manganites continue attracting the attention of condensed matter experts. One of their most intriguing properties is a remarkable response to magnetic fields, the colossal magnetoresistance (CMR), with the dc resistivity changing by more than ten orders of magnitude in some compounds upon the application of a few Tesla.[1,2] Another interesting property, related to the first one, is their rich phase diagrams, with competition of different states, mainly ferromagnetic metallic (FM) phase for $x\sim1/3$, charge-ordered (CO) antiferromagnetic insulating (AFI) phase for $x\sim0.5$, and ferromagnetic insulating (FI) phase for $x\sim0.2$.[3,4] Consequently, they have revealed a remarkable tendency to form heterogeneities observed by a large number of experiments[5,6] and neutron diffraction studies showed a coexistence of long-range magnetic orders.[7] The competition between these different electronic states can be simply understood considering the variation of the level of substitution x, in the framework of the phenomenological Ginsburg-Landau theory.[8,9] When x approaches boundaries between regions of stability of different long-range order phases, fluctuations are enhanced, even at low temperature, and the system becomes highly sensitive to external perturbations such as magnetic field[8] or internal perturbations such as disorder[10] or strains.[11] This can result in a phase separation. Taking advantage of the magnetic contrast between the ferromagnetic (FM and FI) and the nonferromagnetic (AFI) phases in neutron scattering, it was proposed to characterize the sizes of the magnetic heterogeneities by small-angle neutron scattering (SANS). Magnetic heterogeneities observed by this technique were previously reported but they rather spread at the nanometric scale: critical fluctuations around T_C (Ref. 12) and more intriguingly low-temperature nanometric magnetic fluctuations[13] which seemed to decorate the cationic disorder existing in manganites. Their characteristic Q^{-2} SANS scattering can be attributed to magnetic correlations,[14] probably due to electron-phonon coupling.[10]

Since the last decade, the CMR phenomenon is believed to be strongly related, by means of percolation mechanisms, to the tendency of these systems to form inhomogeneous electronic states.[15] For instance, Hardy *et al.*[16] have shown that the insulator-to-metal (I-M) transition characterizing the CMR effect in $Pr_{0.6}Ca_{0.4}MnO_3$ was very well simulated with a percolation law. In this scenario, the magnetic field transforms the CO AFI phase into a FM one, which percolates. They have also shown that the I-M transition is significantly sharper and occurs earlier than predicted by classical three-dimensional (3D) percolation models due to correlations between conducting regions or to an anisotropic geometry of the later.[16]

Since the percolation mechanism implies a continuous transformation, it may appear in contradiction with the first-order character of the CMR transition reported in the literature.[17–20] In particular, Fernandez-Baca *et al.*[19] have shown from inelastic neutron diffraction measurements that the evolution of the spin-wave stiffness at the CMR transition was first order and consequently not consistent with percolation. Despite this apparent contradiction, it has been proposed that a percolative transition can be a first-order transition blurred by disorder or inhomogeneities.[21,22]

In the $Pr_{1-x}Ca_xMnO_3$ series, which show a large variety of states,[4,17] the compositions with $0.3<x<0.4$ are of prime interest because high CMR effects have been observed.[17] Moreover, Pr^{3+} and Ca^{2+} have the same ionic radius,[23] minimizing the cation size mismatch and its consequences on the electronic phase separation. In absence of magnetic field, FI and AFI phases coexist.[7,24] When applying high magnetic field, these phases transform into a FM phase.[16–20]

In order to obtain information concerning magnetic transformations at large scales implied by a percolation scenario, SANS experiments with applied magnetic field were performed on $Pr_{0.7}Ca_{0.3}MnO_3$ crystals.[14,25] The observed magnetic scattering, decreasing monotonously as the magnetic field increased, indicated the existence of nanometric heterogeneities. No increase in the size of these heterogeneities

 ©2010 The American Physical Society

supporting the phase separation at a nanometric scale was observed.[14,25] Besides, by comparing several $Pr_{1-x}Ca_xMnO_3$ samples, with x around 0.3–0.4, it was shown that this scattering signal was directly related to the amount of FI phase in the samples.[14] Finally, we proposed that the magnetic transformation associated to the CMR effect occurs at larger scales (>50 nm),[14] in agreement with high-resolution electron microscopy observations.[5,6] Unfortunately, our experimental setup was limited to a minimum scattering vector Q (the inverse of the typical size observed) of 0.007 $Å^{-1}$, which was too large for a clear quantitative observation of the phenomenon around the I-M transition. Quantitative information was thus still needed on the large scale structure of the phase separation in order to explain the CMR with percolation models. SANS would be the perfect tool, at the condition to reach lower Q values.

The purpose of this paper is to propose a phenomenological description of the colossal magnetoresistance phenomena, based on a study by SANS of the large-scale phase separation in the CMR model compound, $Pr_{0.7}Ca_{0.3}MnO_3$. We have studied the topology of the magnetic phase separation with a good precision from the beginning of the transformation, in the neighboring of the I-M transition, to the metallic ferromagnetic state.

II. EXPERIMENTAL

We have used the SANS spectrometer D22 at ILL, which provides the unique setup to study magnetic heterogeneities down to 0.002 $Å^{-1}$, taking advantage of the large neutron flux available at this Q range while keeping enough scattering signal. The sample was the $Pr_{0.7}Ca_{0.3}MnO_3$ crystal that we have already characterized.[14] It presents 30% of insulating ferromagnetic phase at low temperature (30 K) and in zero magnetic field, the remaining part being antiferromagnetic with charge ordering. No precise orientation of the crystalline axis was chosen, since the CMR effect was found to be isotropic in this sample.[26] A cadmium rectangular diaphragm (9×3.5 mm^2) was put just before the sample to ensure that the neutrons cross the sample over the 2.3 mm of its thickness. The wavelength chosen was 16.52 Å and the sample to detector distance was set to 17.6 m, allowing accessing the scattering vector range 0.002–0.01 $Å^{-1}$. The sample transmission was 0.45. The magnetic field was applied horizontally, perpendicular to the neutron beam. At zero field, the scattering pattern obtained at very low scattering vectors (from 10^{-3} up to around 10^{-2} $Å^{-1}$) was quite anisotropic, probably due to some large scale defects or to the surface itself of the crystal. Application of the magnetic field orientates the magnetic moments parallel to it and concentrates the magnetic scattering observed on the detector in the vertical direction. The intensities were regrouped horizontally and vertically for each value of the scattering vector Q. After subtraction of the background signal obtained without sample, we obtained the sum of the nuclear and the magnetic scattering in the vertical direction, while pure nuclear scattering in the horizontal direction. The subtraction of the nuclear signal is a problem. Indeed, at zero field and low temperature, the SANS signal contains a huge isotropic magnetic signal due to randomly distributed ferromagnetic domains. Moreover a non negligible magnetic SANS signal persists at large Q and high temperature due to local magnetic fluctuations. Finally, the horizontal signal obtained when the magnetization is saturated (at 2 T and above) appears thus as the best possible measurement of the nuclear scattering. The magnetic SANS signal was then obtained by subtracting the horizontal scattering to the vertical one. A calibration factor was applied in order to get the scattering intensity in absolute units (cm^{-1}).[27]

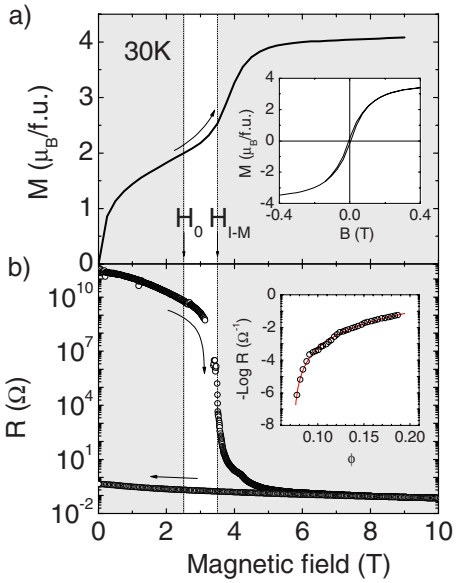

FIG. 1. (Color online) (a) Magnetization and (b) resistance measured for a zero field cooled process at 30 K, showing the colossal magnetoresistive behavior. H_0 marks the beginning of the magnetic transformation around 2.5 T and H_{I-M} marks the I-M transition threshold around 3.5 T. In the inset of Fig. 1(a), a hysteresis cycle of the magnetization is presented after the complete transformation in the ferromagnetic phase, showing the very small hysteresis in this transformed phase. In the inset of Fig. 1(b), the evolution of the conductance versus the ferromagnetic phase fraction deduced from magnetization curve is presented (open circles) together with the simulation with the percolation model (line, red online).

The sample was characterized at 30 K in a Quantum Design physical properties measurement system in conductivity and magnetic modes, under the same experimental conditions as for SANS measurements. For the conductivity measurements, the bias current was carefully regulated to avoid any nonlinearity due to magnetocaloric instabilities and stay in the Ohm's law domain of conductivity.[28]

III. RESULTS AND DISCUSSION

In Fig. 1, the magnetization and the resistance measured vs magnetic field in a zero field cooled process at 30 K are presented. They show the magnetic transformation [from 2.5 T=H_0 to 6 T, Fig. 1(a)] and the insulator-to-metal transition [around 3.5 T=H_{I-M}, Fig. 1(b)] characteristic of the CMR effect. In the inset of Fig. 1(a), we have presented a magnetization cycle of this metallic phase at 30 K. As al-

ready pointed out,[29] after cycling the magnetic field at low temperature, the magnetization returns to zero at zero field. Such an absence of hysteresis[30,31] shows that the ferromagnetic domain walls are not strongly pinned in this compound, compared to what is observed in other ferromagnetic materials. This suggests that the ferromagnetic phase which appears at the CMR transition is fully aligned along the magnetic field, i.e., already at saturation at field around 2 T. An important consequence is that there is no ferromagnetic domain walls, which would give rise to some small-angle signal, at 2 T and over, i.e., along the AFI to FM transformation.

Assuming a percolation process with a conducting ferromagnetic phase fraction ϕ_{FM} given by

$$\phi_{\mathrm{FM}} = \phi - \phi_{\mathrm{FI}} \tag{1}$$

(ϕ being the total amount of ferromagnetism and ϕ_{FI} the amount of ferromagnetic insulating phase), the conductance is expected to vary in the vicinity of the percolation threshold as[32]

$$\frac{1}{R} \propto (\phi_{\mathrm{FM}} - \phi_c)^s. \tag{2}$$

In Eq. (2), ϕ_c is the critical fraction of conducting phase and s a critical exponent characteristic of the sharpness of the transition. The total amount of ferromagnetism ϕ is deduced from the magnetization M, by using

$$M = \phi M_F + (1 - \phi)\chi_{AF} B, \tag{3}$$

where M_F is the saturated magnetization, $(1-\phi)$ is the fraction of AFI, and χ_{AF} its susceptibility. As shown in inset of Fig. 1(b), the fit of the conductance with Eq. (2) in the vicinity of the I-M transition (3.5 T) is very good, supporting the percolation model. The best fit is obtained with ϕ_c close to 7% and s close to 3.5. These values diverge significantly from standard 3D percolation models, which give ϕ_c around 15% and s in the range 1.5–2.[32] This suggests that remarkable properties of the conducting phase make it percolating sooner and more rapidly, such as an elongated geometry or correlations between conducting regions. Similar values of ϕ_c and s have been found in the CMR $Pr_{0.6}Ca_{0.4}MnO_3$ single crystal,[16] which is fully AFI at zero field. This result is important since it demonstrates that the presence of FI phase has no direct influence on the percolation process and thus is not crucial in the CMR mechanism.

In Fig. 2 (filled symbols), we have reported two typical curves of $I(Q)$ obtained at 2 T (before the beginning of the field-induced magnetic transformation) and at 4 T (middle of the transformation) at 30 K after a zero field cooling process. Important variations in the scattering intensity are observed especially at very low Q. Curves exhibit a Q^{-4} law, which is here observed in a broad Q range. This Q^{-4} dependence, shown in Fig. 3(b) in a linear plot $I(Q^{-4})$, is typical of the scattering from sharp interfaces between two media.[33] There is no alternative interpretation for a Q^{-4} scattering. This proves that the magnetic interfaces are sharp. This Q^{-4} scattering is known as the Porod's law

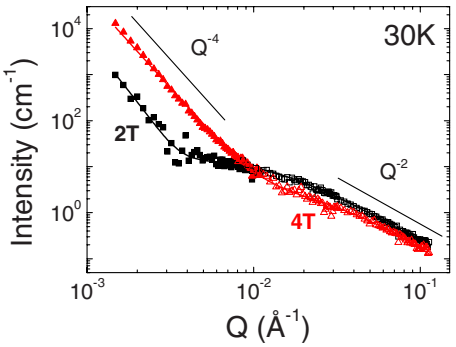

FIG. 2. (Color online) Scattering intensity $I(Q)$ in absolute units at 30 K, for two characteristic magnetic fields: 2 T (squares, black online), before the magnetic transformation begins, and 4 T (triangles, red online), in the middle of the transformation. The data points for $Q > 10^{-2}$ Å^{-1} are precedent SANS measurements obtained on the SANS spectrometer PAXY (LLB, Saclay, France) (Ref. 14). The lines represent the best fits with Eq. (7).

$$I_{Porod}(Q) = 2\pi(\Delta\rho)^2 \frac{S}{V} Q^{-4}, \tag{4}$$

where S/V is the quantity of interfaces between the two media. Here, $\Delta\rho^2$ is the magnetic contrast, the square of the difference of scattering length densities between the ferromagnetic (ρ_{F}) and the nonferromagnetic phases.[34] ρ_{F} was deduced from the magnetization value measured at high field, $M = 3.8\ \mu_{\mathrm{B}}$/unit cell (see Fig. 1). Knowing the scattering length of one μ_{B}, 0.27×10^{-12} cm, and the unit cell volume, 0.57×10^{-22} cm^3, we can deduce the magnetic contrast of our sample: $(\Delta\rho)^2 = 3.24 \times 10^{20}$ cm^{-4}.[14]

According to the lowest Q value, for which we observe the scattering by interfaces, we can first deduce that they belong to ferromagnetic "objects" larger than 100 nm (inverse of Q). The parameter, which can be deduced from $I(Q)$ measured in absolute unit (cm^{-1}), is S/V, the specific area between the two phases. Note that the $I(Q)$ curves overlap perfectly with the previous data[14] obtained for larger Q values (0.007–0.1 Å^{-1}), represented in Fig. 2 as open symbols, in which the Porod's dependence was not clearly observed, especially at low field. In order to ensure the consistency between the present and previous data, S/V has been extracted from the fit of both data, simultaneously, by the same formula [Eq. (7)] in the whole available Q range. For this purpose, Eq. (4), which is valid only in the Q^{-4} Porod's regime, should be changed to be used in a larger Q range, by taking into account a thickness of interfaces.[35] The intensity I_{PS} scattered by the phase separation interfaces can be expressed as

$$I_{PS}(Q) = 2\pi(\Delta\rho)^2 \frac{S}{V} Q^{-4} \exp(-Q^2\sigma^2), \tag{5}$$

where σ is the half width of the interface profile. For $Q \ll 1/\sigma$, the interfaces can be considered as sharp, the intensity follows the Q^{-4} Porod's law of Eq. (4). For $Q \sim 1/\sigma$ and beyond, the intensity should collapse drastically faster than the Q^{-4} Porod's law, as shown in Fig. 4, to further reach a Q^{-8} power law for $Q \gg 1/\sigma$, as discussed by Weissmüller *et*

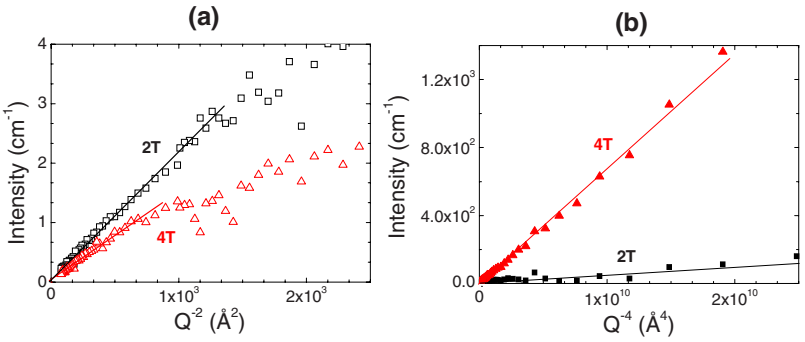

FIG. 3. (Color online) Linear representations of curves shown in Fig. 2 (a) $I(Q^{-2})$ and (b) $I(Q^{-4})$ of same curves. Linear parts indicate (a) a Q^{-2} dependence and (b) a Q^{-4} dependence of the scattering intensities.

al.[36] Such behavior is indeed expected when the observed length scale reaches the order of magnitude of the magnetic coupling length (typically nanometer scale for exchange interactions). The system needs to minimize the local magnetic frustration induced by the two different neighboring magnetic ordered regions. This induces a diffuse magnetic profile of the interface, which should be taken into account for an accurate simulation of the data.

At larger Q range, $0.01 < Q < 0.1$ Å^{-1}, we observe a Q^{-2} scattering intensity (open symbols, Fig. 2), already discussed in a previous paper.[14] Such a variation, clearly observed in the linear representation $I(Q^{-2})$ [Fig. 3(a)], has been interpreted as arising from nanometric magnetic heterogeneities within the initial ferromagnetic insulating phase. Further named I_{nano}, it may be simulated using the scattering function of an aggregate of magnetic fluctuations with a radial distribution of the type $g(r) = \text{Kr}^{-1} \exp(-r/\xi)$ (Ref. 14)

$$I_{\text{nano}}(Q) = A_{\text{nano}} \frac{4}{3} \pi r_0^3 \left[1 + \frac{8\pi K \xi^2}{1 + Q^2 \xi^2} \right] \exp(-Q^2 r_0^2/5), \quad (6)$$

where ξ is the correlation length of the aggregates and r_0 the typical size of the correlated elements. A_{nano} is a factor depending on the quantity and scattering contrast of the magnetic nanometric heterogeneities. The total function that has been used to fit the measured scattered intensity is the sum of Eqs. (5) and (6)

$$I(Q) = 2\pi(\Delta\rho)^2 \frac{S}{V} Q^{-4} \exp(-Q^2\sigma^2) + A_{\text{nano}} \frac{4}{3} \pi r_0^3 \left[1 + \frac{8\pi K \xi^2}{1 + Q^2 \xi^2} \right] \exp(-Q^2 r_0^2/5). \quad (7)$$

Typical fits with Eqs. (5)–(7) are shown in Fig. 4 for applied field of 2 and 4 T: there is a good agreement between experimental data and fits with Eq. (7) (lines). The best fits parameters are listed in Table I. Note that the Q^{-4} power law is observed here on a sufficiently broad Q range so that the fit with Eq. (4) would be enough to determine accurate values of S/V in the right Porod's Q range. Moreover, in this range, it gives the same S/V values, within error bars, that Eq. (7) in the whole Q range. Similarly, A_{nano} deduced from the fit with Eq. (7) equals the value extracted from the previous data.[14] As a matter of fact, $I_{PS}(Q)$ and $I_{\text{nano}}(Q)$ concern very different "object" sizes and thus influence the scattering intensity $I(Q)$ in distinct and limited Q ranges (Fig. 4): the Q^{-4} signal from the phase separation rapidly falls to zero vs Q while the signal arising from the nanometric fluctuations of the remaining FI phase has not yet decreased. So, though Eq. (7) contains a lot of variables, the quantitative information extracted from the fit with this equation is trustworthy.

The evolution of the specific area S/V of the large-scale phase separation and the A_{nano} factor of the nanometric scattering arising from the FI phase are shown in Fig. 5. By using the magnetic contrast ($\Delta\rho^2 = 3.24 \times 10^{20}$ cm^{-4}), we obtain values of S/V in between 0.05 and 0.5 μm^{-1}. Moreover, as already observed, the constant decrease of A_{nano}, the factor depending on the quantity and scattering contrast of magnetic nanometric heterogeneities, allows us to definitively dismiss the percolation of nanometric objects at the I-M transition. In contrast, S/V increases as the magnetic transformation begins (2.5 T, dotted line in Fig. 5). It then reaches a maximum at 4.7 T and finally decreases above this field. This is exactly what is expected in the case of a nucleation of ferromagnetic clusters growing in an antiferromagnetic matrix, percolating to eventually fill the whole volume. Similar variations in S/V, not shown here, have been obtained in another crystal of slightly different composition, $Pr_{0.66}Ca_{0.34}MnO_3$, which also displayed a CMR effect.[14]

These continuous variations in S/V obviously support the percolation scenario, while Fernandez-Baca *et al.*,[19] which

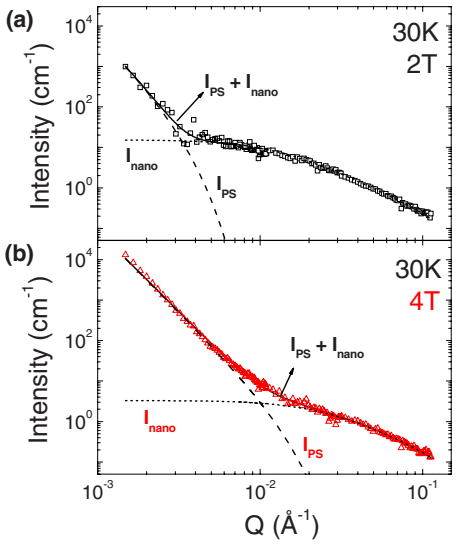

FIG. 4. (Color online) Scattering intensity $I(Q)$ in absolute units at 30 K for applied fields of (a) 2 T and (b) 4 T. Lines are best fits to Eq. (7) ($I_{PS}+I_{\text{nano}}$). Dotted and dashed lines are fits to Eq. (5) (I_{PS}) and Eq. (6) (I_{nano}), respectively.

TABLE I. Variations as a function of the applied magnetic field of the best fit parameters with Eq. (7) of the magnetic SANS. S/V is the total specific area between the growing FM phase inside the AF phase, σ is the half width of the profile between these two phases. A_{nano} is a prefactor, which represents the amount of nanometric fluctuations inside the FI phase and ξ is the correlation length of these fluctuations. The parameters K and r_0 have been set constant for all the fits: $K \sim 4.1 \times 10^{-4} \pm 1.7 \times 10^{-4}$ Å^{-2}. $r_0 \sim 17 \pm 3$ Å. * indicates values interpolated from the neighboring fit parameters. R is the correlation coefficient between experimental data and calculated values.

Magnetic field (T)	S/V (μm^{-1})	σ (μm)	A_{nano} (cm^{-1} Å^{-3})	ξ (Å)	R
2.0	0.041 ± 0.006	0.035 ± 0.003	$5.0 \pm 0.1 \times 10^{-5}$	79 ± 2	0.989
2.5	0.052 ± 0.007	0.027 ± 0.003	5.0×10^{-5}*	79*	0.969
2.75	0.066 ± 0.006	0.021 ± 0.002	5.0×10^{-5}*	79*	0.981
3.0	0.091 ± 0.009	0.017 ± 0.003	$5.0 \pm 0.1 \times 10^{-5}$	79 ± 4	0.993
3.25	0.138 ± 0.008	0.015 ± 0.002	5.0×10^{-5}*	76*	0.994
3.5	0.197 ± 0.012	0.012 ± 0.002	$5.0 \pm 0.1 \times 10^{-5}$	70 ± 5	0.997
3.75	0.242 ± 0.009	0.007 ± 0.001	4.0×10^{-5}*	63*	0.995
4.0	0.382 ± 0.010	0.006 ± 0.0015	$3.0 \pm 0.1 \times 10^{-5}$	61 ± 5	0.998
4.25	0.448 ± 0.011	0.0055 ± 0.0005	3.0×10^{-5}*	47*	0.998
4.5	0.503 ± 0.019	0.004 ± 0.001	$2.0 \pm 0.05 \times 10^{-5}$	40 ± 6	0.998
4.75	0.522 ± 0.012	0.005 ± 0.0005	1.0×10^{-5}*	30*	0.998
5.0	0.486 ± 0.026	0.002 ± 0.003	$6.8 \pm 0.6 \times 10^{-6}$	24 ± 10	0.997
5.5	0.484 ± 0.011	0.0055 ± 0.0005	6.0×10^{-6}*	14*	0.998
6.0	0.328 ± 0.020	0.0015 ± 0.001	$5.7 \pm 0.5 \times 10^{-6}$	6 ± 3	0.992
6.5	0.163 ± 0.004				

observed first order characteristics, excluded this hypothesis. These authors have measured by inelastic neutron diffraction a small spin-wave stiffness below 3 T, when insulating, and a high one above 3.5 T, when conducting. Their first main argument against the percolation scenario was that the spin-wave stiffness should be high due to the conducting clusters all along the percolation while it was small below 3 T. The magnetization curve (Fig. 1) shows that the magnetic transformation is very narrow (at 3.5 T for our sample), but monotonous and has not yet started at 2.5 T, in good agreement with the small spin-wave stiffness constant measured at 3 T by Fernandez Baca *et al.*[19] Moreover, it is clearly seen from Figs. 1 and 5 that 3.5 T is just in the core of the magnetic transformation, again in good agreement with the high spin-wave stiffness constant at 3.5 T.

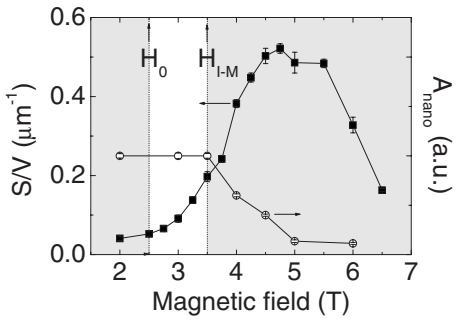

FIG. 5. Evolution versus magnetic field of the specific area (S/V) of abrupt interfaces between two phases at 30 K and the factor A_{nano} of the nanometric scattering, deduced from the fit of the $I(Q)$ curves with Eq. (7). H_0 marks the beginning of the magnetic transformation around 2.5 T [from magnetization curve, Fig. 1(a)] and $H_{I\text{-}M}$ marks the I-M transition threshold around 3.5 T [deduced from $R(H)$ curve, Fig. 1(b)].

A first-order transition is often proposed for the CMR effect,[18,19,37] which is consistent with the irreversible changes that we observe here [both $M(H)$ and $R(H)$ plots in Fig. 1 show that the system does not turn back to AF when the magnetic field is switched off]. It makes impossible to have energetically favorable intermediate homogeneous state between initial and final ones, and can thus lead to phase separation. Moreover, Li *et al.*[37] demonstrated that first-order transitions tend to be a general rule of strongly coupled magnetic-conductive transitions, such as CMR in manganites. Nevertheless, our observations show a continuous evolution at the microscopic scale of FM phase and Dagotto *et al.*[21] have demonstrated that percolative transitions in CMR manganites can be the consequence of disorder near a first order I-M transition. The continuous transitions observed at large scale are most likely the consequence of the smearing of the first-order transformation by disorder[22] because local disorder induces a distribution of subsystems that would not start transforming at the same field. The percolative evolution observed here can thus be simply viewed as the microscopic feature of locally, and not explored by SANS, first-order transitions.

In order to get further insight into the micrometric phase separation observed here, we have deduced a characteristic size $\langle l \rangle$ of this phase separation from S/V, using the general relation demonstrated by Porod[33]

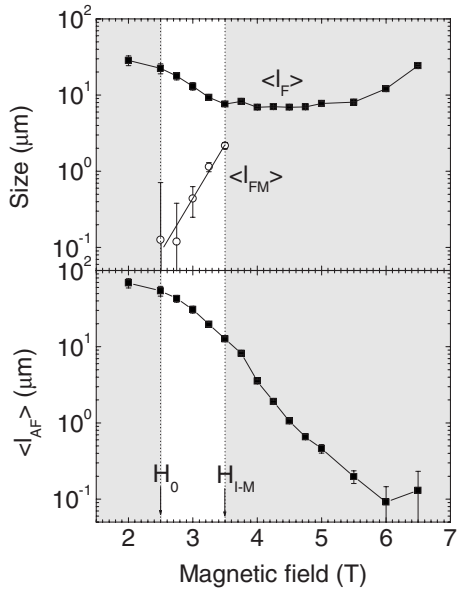

FIG. 6. Evolutions of the average sizes of (a) ferromagnetism $\langle l_F \rangle$ (insulating ferromagnetism FI and field induced conducting FM) and conducting FM $\langle l_{FM} \rangle$, and (b) AFI $\langle l_{AF} \rangle$, deduced from Eqs. (9), (11), and (10), respectively.

$$\frac{S}{V} = \frac{4\phi(1-\phi)}{\langle l \rangle}. \tag{8}$$

Here, ϕ and $(1-\phi)$ are the fractions of ferromagnetism (initial insulating ferromagnetism and field induced metallic ferromagnetism) and initial antiferromagnetism, respectively, as deduced from the magnetization curve using Eq. (3). The corresponding ferromagnetic and antiferromagnetic mean sizes $\langle l_F \rangle$ and $\langle l_{AF} \rangle$ can be deduced from $\langle l \rangle$, using[33]

$$\langle l_F \rangle = \frac{\langle l \rangle}{1-\phi}, \tag{9}$$

$$\langle l_{AF} \rangle = \frac{\langle l \rangle}{\phi}. \tag{10}$$

They are represented versus applied magnetic field in Fig. 6.

At 2 T, $\langle l_F \rangle$ and $\langle l_{AF} \rangle$, the sizes of the initial large scale FI/AFI magnetic phase separation, are 23 μm and 55 μm, respectively. These sizes are too large to be due to Coulomb or other electrostatic interactions. They are also significantly larger than possible phase separation due to cationic disorder according to the simulations of Moreo *et al.*,[10,38] which should rather lie in the mesoscopic range scale. Such large-scale phase separation suggests that the separated phases correspond to energetically close electronic states and that the main mechanism that governs the topology is the minimization of the interface energy. The later must originate from the known elastic mismatch between crystalline structures.[7] This suggests that the topology of the initial phase separation is governed by strain minimization.

At the very beginning of the transformation, from 2.5 to 3.5 T, it is clearly seen that the average size $\langle l_F \rangle$ of the ferromagnetic domains decreases, whereas we know from Fig. 5 that the fluctuations in the initial FI phase are not yet affected (since A_{nano} remains constant). This shows that the nucleation of metallic ferromagnetic regions first occurs in the initial AFI phase. The size of these FM regions [open circles on Fig. 6(b)] can be deduced by replacing, in Eqs. (8) and (9), S/V and ϕ by $\Delta S/V = S/V - S/V_{2\ \text{T}}$ and ϕ_{FM}, respectively,

$$\langle l_{\text{FM}} \rangle = \frac{4\phi_{\text{FM}}}{\Delta S/V}. \tag{11}$$

The FM phase fraction ϕ_{FM} is calculated from Eq. (3) taking ϕ_{FI} constant (since not yet affected at low fields), i.e., equals to 30%. The average size of these FM regions $\langle l_{\text{FM}} \rangle$, initially around 100 nm at 2.5 T (see Fig. 6), increases exponentially with the magnetic field. The transformation occurs by nucleation and growth of mesoscopic (100–1000 nm) ferromagnetic conducting regions. This range of size typically corresponds to what Moreo *et al.*[38] predicted for disordered-induced phase separation. This suggests that disorder-induced heterogeneities could constitute nucleation centers of FM phase within the AFI phase when an external magnetic field is applied.

Concerning the core of the transformation, from 3.5 to 5.5 T, the average size $\langle l_F \rangle$ of the ferromagnetic domains remains constant [Fig. 6(a)], equals to 8 μm, while the mean size of the initial AFI phase $\langle l_{AF} \rangle$ decreases drastically [Fig. 6(b)]. As previously proposed,[39] in this range of magnetic field, the transformation is also governed by strain minimization, since, as for the initial FI/AFI phases, FI and FM phases also have different unit-cell parameters.[7] The nucleation and growth of FM clusters within the AFI phase must induce the apparition and rising of an elastic strain field. The characteristic size of about 8 μm of the FM regions, reached at 3.5 T, is probably the size at which it becomes energetically favorable to reduce the amount of FI phase in order to minimize the large scale strain field induced by the growth of the FM phase. This size of 8 μm probably corresponds to an optimum between the interface elastic energy and the energy difference between separated electronic states.

The threshold between these two mechanisms of transformation (3.5 T) is also the threshold of the I-M transition associated with the CMR effect. Therefore, the percolation occurs when the large scale strain field becomes a major parameter of the magnetic transformation. We are thus tempted to propose that it is the reason why the percolation occurs earlier and is sharper than predicted by standard non-correlated 3D percolation models. The general trend seems to be that the more the transformation is governed by strains, the sharper the percolative insulator-to-metal transition. This is consistent with the fact that at lower temperature (<5 K), the I-M transition occurs as a steplike jump,[39] which is typical of a transformation mechanism governed by strain field minimization.[40]

IV. CONCLUSION

By extending the Q range of the SANS study down to 0.002 Å^{-1}, we have been able to depict the complex and multiscale topology of heterogeneities in the CMR mangan-

ites, from the beginning of the magnetic field-induced transformation up to the vicinity of the I-M transition. The initial insulating phase separation (FI/AFI) has been found to be in the $20-60\mu$ range, i.e., too large to be related to cationic disorder, suggesting that separated initial electronic states are close in energy while the interface elastic energy minimization governs the topology. When applying an external magnetic field, the magnetic transformation associated with the CMR effect has been found to occur by nucleation and growth of mesoscopic FM regions. We have shown that the I-M transition is induced by the percolation of these FM regions. This percolative transition is nonetheless significantly sharper than standard 3D percolation models that do not take into account interactions between conducting regions. Moreover, we have shown that the I-M transition occurs when the transformation mechanism starts to be driven by large scale strain field minimization. We conclude that the remarkable sharpness of the I-M transitions observed in these low-temperature CMR manganites is the consequence of large-scale strains between coexisting phases.

*Corresponding author; charles.simon@ensicaen.fr

[1] For a review, see, for example, J. M. D. Coey, M. Viret, and S. von Molnar, Adv. Phys. **48**, 167 (1999); *Colossal Magnetoresistance, Charge Ordering and Related Properties of Manganese Oxides*, edited by C. N. R. Rao and B. Raveau (World Scientific, Singapore, 1998); *Colossal Magnetoresistance Oxides*, edited by Y. Tokura (Gordon and Breach, New York, 1998).

[2] B. Raveau, A. Maignan, and V. Caignaert, J. Solid State Chem. **117**, 424 (1995).

[3] K. Tobe, T. Kimura, and Y. Tokura, Phys. Rev. B **69**, 014407 (2004).

[4] C. Martin, A. Maignan, M. Hervieu, and B. Raveau, Phys. Rev. B **60**, 12191 (1999).

[5] M. Uehara, S. Mori, C. H. Chen, and S.-W. Cheong, Nature (London) **399**, 560 (1999).

[6] M. Fäth, S. Freisem, A. A. Menovsky, Y. Tomioka, J. Aarts, and J. A. Mydosh, Science **285**, 1540 (1999).

[7] P. G. Radaelli, R. M. Ibberson, D. N. Argyriou, H. Casalta, K. H. Andersen, S.-W. Cheong, and J. F. Mitchell, Phys. Rev. B **63**, 172419 (2001).

[8] S. Murakami and N. Nagaosa, Phys. Rev. Lett. **90**, 197201 (2003).

[9] G. C. Milward, M. J. Calderon, and P. B. Littlewood, Nature (London) **433**, 607 (2005).

[10] J. Burgy, A. Moreo, and E. Dagotto, Phys. Rev. Lett. **92**, 097202 (2004).

[11] K. H. Ahn, T. Lookman, and A. R. Bishop, Nature (London) **428**, 401 (2004).

[12] J. M. De Teresa, M. R. Ibarra, P. A. Algarabel, C. Ritter, C. Marquina, J. Blasco, J. Garca, A. del Moral, and Z. Arnold, Nature (London) **386**, 256 (1997).

[13] Ch. Simon, S. Mercone, N. Guiblin, C. Martin, A. Brûlet, and G. André, Phys. Rev. Lett. **89**, 207202 (2002).

[14] D. Saurel, A. Brûlet, A. Heinemann, C. Martin, S. Mercone, and Ch. Simon, Phys. Rev. B **73**, 094438 (2006).

[15] E. Dagotto, Science **309**, 257 (2005).

[16] V. Hardy, A. Wahl, and C. Martin, Phys. Rev. B **64**, 064402 (2001).

[17] Y. Tomioka, A. Asamitsu, H. Kuwahara, Y. Moritomo, and Y. Tokura, Phys. Rev. B **53**, R1689 (1996).

[18] M. Roy, J. F. Mitchell, A. P. Ramirez, and P. Schiffer, Phys. Rev. B **62**, 13876 (2000).

[19] J. A. Fernandez-Baca, P. Dai, H. Kawano-Furukawa, H. Yoshizawa, E. W. Plummer, S. Katano, Y. Tomioka, and Y. Tokura, Phys. Rev. B **66**, 054434 (2002).

[20] A. Anane, J. P. Renard, L. Reversat, C. Dupas, P. Veillet, M. Viret, L. Pinsard, and A. Revcolevschi, Phys. Rev. B **59**, 77 (1999).

[21] E. Dagotto, T. Hotta, and A. Moreo, Phys. Rep. **344**, 1 (2001).

[22] C. Şen, G. Alvarez, and E. Dagotto, Phys. Rev. B **70**, 064428 (2004).

[23] R. D. Shannon, Acta Crystallogr. **32**, 751 (1976).

[24] D. E. Cox, P. G. Radaelli, M. Marezio, and S.-W. Cheong, Phys. Rev. B **57**, 3305 (1998).

[25] M. Viret, F. Ott, J. P. Renard, H. Glättli, L. Pinsard-Gaudart, and A. Revcolevschi, Phys. Rev. Lett. **93**, 217402 (2004).

[26] S. Mercone, V. Hardy, C. Martin, Ch. Simon, D. Saurel and Annie Brûlet, Phys. Rev. B **68**, 094422 (2003).

[27] J. P. Cotton, in *Neutron, X-ray and Light Scattering*, edited by P. Lindner and Th. Zemb (North-Holland, Amsterdam, 1991), p. 19.

[28] S. Mercone, R. Frésard, V. Caignaert, C. Martin, D. Saurel, Ch. Simon, G. André, P. Monod, and F. Fauth, J. Appl. Phys. **98**, 023911 (2005).

[29] Y. Tokura and Y. Tomioka, J. Magn. Magn. Mater. **200**, 1 (1999).

[30] A. Maignan, Ch. Simon, V. Caignaert, and B. Raveau, Z. Phys. B **99**, 305 (1996).

[31] J. Wolfman, M. Hervieu, and Ch. Simon, Nucl. Instrum. Methods Phys. Res. B **179**, 176 (2001).

[32] S. Kirkpatrick, Rev. Mod. Phys. **45**, 574 (1973).

[33] G. Porod, in *Small Angle X-ray Scattering*, edited by O. Glatter and O. Kratky (Academic Press, London, 1983), p. 35.

[34] Damien Saurel, the average magnetic moment of atoms inside an antiferromagnetic cell is zero at the scale observed by SANS ($1/Q > 8$ Å).

[35] M.-H. Kim, J. Appl. Crystallogr. **37**, 643 (2004).

[36] J. Weissmüller, R. D. McMichael, A. Michels, and R. D. Shull, J. Res. Natl. Inst. Stand. Technol. **104**, 261 (1999).

[37] Q. A. Li, K. E. Gray, S. N. Ancona, H. Zheng, S. Rosenkranz, R. Osborn, and J. F. Mitchell, Phys. Rev. Lett. **96**, 087201 (2006).

[38] A. Moreo, M. Mayr, A. Feiguin, S. Yunoki, and E. Dagotto, Phys. Rev. Lett. **84**, 5568 (2000).

[39] D. Saurel, Ch. Simon, A. Brûlet, A. Heinemann, and C. Martin, Phys. Rev. B **75**, 184442 (2007).

[40] V. Hardy, S. Majumdar, S. Crowe, M. R. Lees, D. Mc. Paul, L. Hervé, A. Maignan, S. Hébert, C. Martin, C. Yaicle, M. Hervieu, and B. Raveau, Phys. Rev. B **69**, 020407 (2004).